

Publication information

Title	Reactive Oxygen Species Production Mediated by Humic-like Substances in Atmospheric Aerosols: Enhancement Effects by Pyridine, Imidazole, and Their Derivatives
Author(s)	Dou, Jing; Lin, Peng; Kuang, Bin-Yu; Yu, Jian Zhen
Source	Environmental Science and Technology , v. 49, (11), June 2015, p. 6457-6465
Version	Published version
DOI	https://doi.org/10.1021/es5059378
Publisher	American Chemical Society

Copyright information

© 2015 American Chemical Society

Notice

This version is available at HKUST Institutional Repository via

<http://hdl.handle.net/1783.1/71245>

If it is the author's pre-published version, changes introduced as a result of publishing processes such as copy-editing and formatting may not be reflected in this document. For a definitive version of this work, please refer to the published version.

1 **Reactive Oxygen Species production mediated by Humic-like substances in**
2 **Atmospheric Aerosols: Enhancement effects by pyridine, imidazole and their**
3 **derivatives**

4 Jing Dou¹, Peng Lin^{2,#}, Bin-Yu Kuang², Jian Zhen Yu^{1,2,*}

5 ¹Division of Environment, Hong Kong University of Science & Technology, Clear Water
6 Bay, Kowloon, Hong Kong, China

7 ²Department of Chemistry, Hong Kong University of Science & Technology, Clear Water
8 Bay, Kowloon, Hong Kong, China

9 [#]now at Environmental Molecular Sciences Laboratory, Pacific Northwest National
10 Laboratory, Richland, Washington, WA99532,

11 *Corresponding author: jian.yu@ust.hk

12
13 **Abstract**

14 Ambient particulate matter (PM) can cause adverse health effects via their ability to produce
15 reactive oxygen species (ROS). Humic-like substances (HULIS), a complex mixture of
16 amphiphilic organic compounds, have been demonstrated to contain the majority of redox
17 activity in the water-extractable organic fraction of PM. Reduced organic nitrogen
18 compounds, such as alkaloids resulting from biomass burning emissions, are among HULIS
19 constituents. In this study, we examined the redox activities of pyridine, imidazole and their
20 alkyl derivatives (i.e., 3-methoxypyridine, 4-methylimidazole, 2-methylimidazole, and 2,4-
21 dimethylimidazole) using a cell-free dithiothreitol (DTT) assay under simulated physiological
22 conditions (37°C, pH =7.40). These compounds were found to not have redox activity on
23 their own as measured by the DTT assay, but they enhanced ROS generation catalyzed by
24 1,4-naphthoquinone (as a model quinone compound) and HULIS isolated from multiple
25 aerosol samples. The enhancement effect by the individual nitrogen-containing bases was
26 determined to be proportional to their amount in the assay solutions. It is postulated that the
27 underlying mechanism involves the unprotonated N atom acting as a H-bonding acceptor to

28 facilitate hydrogen-atom transfer in the ROS generation cycle. The enhancement capability
29 was found to increase with their basicity (i.e., pK_a of their conjugated acids, BH^+), consistent
30 with the proposed mechanism for enhancement. Among the imidazole homologues, a linear
31 relationship (log scale) was observed between the enhancement factors of the unprotonated
32 form of the imidazole compounds (i.e., B) and the pK_a of their conjugated acids (i.e., BH^+).
33 This relationship predicts that the range of alkyl imidazole homologues (C_6 - C_{13}) observed in
34 atmospheric HULIS would be 1.6-5 times more effective than imidazole in facilitating
35 HULIS-mediated ROS generation. Our work reveals that the ability of atmospheric PM
36 organics to catalyze generation of ROS in cells could be affected by co-existing redox
37 inactive organic constituents and highlights the importance in identifying and quantifying the
38 individual redox active constituents as well as the redox inactive nitrogen-containing bases.

39 **Key words:** Organic Aerosols, Health Effect, Reactive Oxygen Species, alkaloids

40

41 **Introduction**

42 Ambient particulate matter (PM) is an important air pollutant known to cause adverse
43 health effects and mortality in humans.¹⁻³ One of the major toxicological mechanisms is
44 through the induction of oxidative stress derived from PM-mediated generation of reactive
45 oxygen species (ROS) in cells.⁴⁻⁷ Among the numerous constituents of PM, metals⁸⁻¹² and
46 quinoid compounds¹³ have been established as capable of catalyzing ROS generation in cells.
47 More recently, humic-like substances (HULIS), a complex mixture of water-extractable
48 amphiphilic organic compounds having structural similarities to terrestrial and aquatic humic
49 substances (HS),¹⁴ have also been recognized as major redox-active components in ambient
50 PM and can serve as electron carriers to catalyze ROS formation.^{15,16} However, the specific
51 components of HULIS that impact ROS formation activity have been largely unexplored.

52 Our previous ultra-high resolution mass spectrometric (UHRMS) study identified

53 nitrogen-containing heterocyclic compounds of double bond equivalency (DBE) 3 or 4 (i.e.,
54 alkaloids) among the most abundant peaks detected under positive electrospray ionization
55 mode in the HULIS fraction of ambient and biomass burning (BB) source samples collected
56 in the Pearl River Delta (PRD) region of China.¹⁷ Laskin et al.¹⁸ also reported alkaloid
57 compounds as abundant constituents in aerosols emitted from various biofuels. Alkaloids are
58 generally basic compounds derived from amino acids in plants and living organisms, and can
59 be emitted from smoldering fires with minor pyrolytic and oxidative processing.¹⁹
60 Additionally, some alkaloids, such as imidazole, imidazole-2-carboxaldehyde and 1N-
61 glyoxal-substituted imidazole, are also reported to be major products of glyoxal reaction with
62 ammonium ions or primary amines on secondary organic aerosol (SOA).²⁰⁻²²

63 The dithiothreitol (DTT) assay is a chemical method developed for evaluating the
64 redox cycling capacity of catalytically active redox species by measuring how fast DTT is
65 oxidized.²³ In this study, we initially hypothesized that the lone pair of electrons in alkaloid
66 compounds might render them to be redox-active. A few alkaloids (e.g., imidazole, pyrrole,
67 pyridine, pyrimidine, pyrazine and their derivatives) were tested by the DTT assay, but all
68 showed negligible ROS activity. Prompted by the Kipp et al.²⁴ cyclic voltammetry study that
69 showed unprotonated imidazole can accept a proton from the reductant, facilitating electron
70 transfer, we experimented both a DTT assay of a redox-active model compound (e.g.
71 quinones) and atmospheric HULIS samples in the presence of atmospheric relevant alkaloids
72 (i.e., imidazole, pyridine, and some of their derivatives). The results indicate that they could
73 facilitate the production of ROS. Figure 1 shows a conceptual diagram of alkaloids forming
74 H-bonding with a hydroquinone compound (as a model ROS-active compound) and
75 concomitant consumption of DTT. In the presence of these nitrogen-containing compounds,
76 the oxidation of organic compounds that normally lose hydrogen atoms could be enhanced by
77 the formation of H-bonding.

78

79 **Experimental Section**

80 **Aerosol Samples.** Ambient samples of PM_{2.5} (PM of less than 2.5 μm in aerodynamic
81 diameter) were collected at urban (Guangzhou (GZ)) and suburban (Nansha (NS)) locations
82 in the PRD of in 2009. The samples were collected onto prebaked quartz filters using a high
83 volume aerosol sampler (TE-6070 V-BL, Tisch Environmental Inc., USA). The sampling
84 duration for individual samples was 24 h.

85 Fresh BB emissions samples were collected from open burning experiments in a village.
86 Locally harvested rice straw in small bundles and sugar cane leaves in thin piles were burned,
87 simulating the open field burning practiced by farmers. PM_{2.5} smoke particles were collected
88 about 5 m downwind of the fires. More details about the sampling work can be found in our
89 previous papers.^{25,26}

90 **HULIS Isolation and Determination.** HULIS in aerosol filter samples was first isolated
91 from the other constituents in water extracts using solid phase extraction (SPE), followed by
92 quantification by an evaporative light scattering detector (ELSD). The isolation procedure
93 separates the water-soluble matter into a hydrophilic fraction (the SPE cartridge effluent) and
94 a hydrophobic fraction (i.e., the HULIS fraction or the eluate fraction). In brief, portions of
95 the high-volume filters were extracted in an ultrasonic bath with water, the volume of which
96 used was about 1 mL per 1 cm² filter area for extraction. The extract was acidified with HCl
97 (pH 2) before it was loaded on a SPE cartridge (Oasis HLB, 30 μm, 60 mg/cartridge, Waters),
98 with the ratio of HCl to the extract set to be ~ 4 μL per mL. The loaded cartridge was
99 subsequently rinsed with two 1 mL portions of water before elution with 12 mL methanol.
100 The eluate was collected and evaporated to dryness under a gentle stream of N₂ and resolved
101 in water for HULIS quantification and DTT assay. Details on the characteristics and
102 performance of this method have been reported in our previous work.²⁵ It should be noted

103 that in this work 12 mL of methanol instead of 1.5 mL of methanol containing 2% ammonia
104 was used as the elution solvent. This alteration was to avoid possible chemical modification
105 of the HULIS fraction as ammonia may react with carbonyl compounds to generate imines.²⁷
106 The increased volume of elution solvent was to ensure satisfactory elution efficiency.¹⁵

107 **DTT Assay.** DTT, diethylene triamine pentaacetic acid (DTPA), 1,4-naphthoquinone
108 (1,4-NQ), 5,5'-dithio-bis(2-nitrobenzoic acid) (DTNB), 3-methoxypyridine, pyridine,
109 imidazole, 4-methylimidazole and 2-methylimidazole were obtained from Sigma Chemical
110 Co. (St. Louis, MO). 2,4-dimethylimidazole was purchased from Meryer Chemical
111 Technology Co., Ltd. (China).

112 The procedure of the DTT assay in this study follows that used by Lin and Yu.¹⁵
113 Briefly, 200 μL of sample aliquot was first mixed with 950 μL of 0.1 M potassium phosphate
114 buffer (pH 7.40) containing 1 mM DTPA. DTPA was added to the phosphate buffer to inhibit
115 DTT consumption by metal ions.²⁸ The composition of each 200 μL sample aliquot varied
116 across the tests, as shown in Table 1. A 50 μL aliquot of 0.5 mM DTT solution was then
117 added and the mixture was allowed to react at 37°C in an oven for 30 min in 1,4-NQ
118 experiments, or 90 min in HULIS experiments, or 30 min in experiments involving both 1,4-
119 NQ and HULIS. A 100 μL solution of 1.0 mM DTNB (dissolved in 0.1 M potassium
120 phosphate buffer containing 1 mM DTPA) was added to the reaction solution to generate a
121 colored product. Absorption (A) measurements at 412 nm were taken using a diode-array
122 spectrophotometer within 30 min. Each experiment of the DTT assay was run in triplicate.

123 The DTT assay response (R_{DTT}), defined as the percentage of DTT consumed, is
124 computed using the equation below:

$$125 \quad R_{\text{DTT}} = \frac{A_0 - A}{A_0} \times 100\% \quad (1)$$

126 where A_0 is the absorbance due to DTT added in a blank sample and A is the absorbance due

127 to DTT added in a sample. In the blank sample, DTT is only consumed by dissolved O₂. The
 128 calibration curve confirmed that absorbance is linearly proportional to the DTT
 129 concentrations in the solution ($R^2 > 0.99$). The rate of DTT consumption in picomole per
 130 minute of incubation time per microgram of ROS active component (i.e., pmol/ min/ μ g) is
 131 then calculated with Eq (2):

$$132 \quad \Delta DTT(\text{pmol} / \text{min} / \mu\text{g}) = \frac{R_{\text{DTT}}}{t \times m} \times n_{\text{DTT}} \quad (2)$$

133 where t is the reaction time (min), m is the mass of ROS-active component (1,4-NQ or
 134 HULIS) (μ g), and n_{DTT} is the amount of DTT added in the tube (pmol). The DTT assay
 135 performed on samples containing each of the six tested alkaloid compounds verified that they
 136 have no DTT activity on their own.

137

138 **Results and Discussion**

139 **Detection of Nitrogen-containing Compounds.** The presence of imidazole, pyridine
 140 and their derivatives in atmospheric HULIS samples was checked using ultra-high resolution
 141 mass spectrometric (UHRMS) data obtained in positive electrospray ionization (ESI+) mode.
 142 One ambient sample and two BB source samples were extracted and treated to obtain the
 143 HULIS fraction followed by analysis using Fourier transform ion cyclotron resonance mass
 144 spectrometry (FT-ICR MS). The m/z values were normalized to CH₂ to get the Kendrick
 145 mass²⁹ using Eq (3):

$$146 \quad \text{Kendrick mass} = (\text{exact } m/z \text{ value of peak}) \times (14/14.01565) \quad (3)$$

147 Then Kendrick Mass Defect (KMD) of the peak is calculated with Eq (4):

$$148 \quad \text{KMD} = \text{nominal Kendrick mass} - \text{exact Kendrick mass} \quad (4)$$

149 Homologous series that differ by the CH₂ groups have an identical KMD value.³⁰ Figure S1
 150 shows the plots of KMD versus carbon numbers for compounds containing one N and two N
 151 atoms (abbreviated as N₁ and N₂ compounds hereafter) in the HULIS fraction of ambient,

152 rice straw burning and sugar cane leaves burning aerosol samples collected in the PRD region.
153 The signal-to-noise ratio values are color-coded to indicate their relative abundances within
154 the same sample. The N_1 formulas with $KMD = 0.046$ represent the homologues of pyridine,
155 while the N_2 formulas with $KMD = 0.0385$ represent the homologues of imidazole. The C_7 -
156 C_{14} homologues of pyridine and the C_7 - C_{13} homologues of imidazole were detected in the
157 HULIS fraction of the BB aerosols. Out of those detected in the source samples, three
158 imidazole homologues and seven pyridine homologues were also detected in the ambient
159 HULIS sample. Higher abundance was found in the BB source samples (rice straw and sugar
160 cane samples), which may be attributed to the phenomenon that smoldering fire is typical
161 burning condition for rice straw in the PRD region.¹⁷ The UHRMS data, although not
162 definitive evidence for the identification of these N_1 and N_2 series compounds as imidazole
163 and pyridine derivatives, strongly suggests their plausible presence in ambient atmospheric
164 aerosols.

165 **Enhancement of 1,4-NQ ROS activity by HULIS.** The hypothesis that the nitrogen-
166 containing bases (N-bases) in alkaloids could enhance the ROS activity of ROS-reactive
167 organic compounds was first tested by examining the mixture of 1,4-NQ (serving as a model
168 ROS-reactive compound) and HULIS (which contains the N-bases with perceived ROS
169 enhancing capability). The DTT consumption by the mixture of 1,4-NQ and HULIS was
170 measured and compared with those measured for the same amount of 1,4-NQ (3 $\mu\text{g}/\text{mL}$) and
171 HULIS (60 $\mu\text{g}/\text{mL}$) in separate solutions. One ambient HULIS sample (NS20091023) and
172 one HULIS sample from rice straw burning were used in this set of experiments and the
173 results are shown in Figure 2. It is clear that the DTT response from the mixture of 1,4-NQ
174 and HULIS was more than the sum of individual responses, where the mixture with ambient
175 HULIS is 3.8 % greater and the mixture with rice straw burning HULIS is 33.2 % greater
176 than the individual responses. The DDT consumption rate by 1,4-NQ was 727 ± 30

177 pmol/min/ μg in the absence of HULIS, but this value increased to 831 ± 45 pmol/min/ μg in
178 the presence of 6 μg ambient HULIS and 1649 ± 75 pmol/min/ μg in the presence of 6 μg BB
179 source HULIS. The DDT consumption rate by 1,4-NQ in the mixture was calculated by
180 deducting the DDT consumption due to HULIS. The results indicate that certain compounds
181 in HULIS could enhance the 1,4-NQ redox activity to generate ROS. The larger enhancement
182 elicited by the BB source HULIS is consistent with the higher abundance of N-base
183 compounds in the BB source samples than the ambient sample.

184 **Enhancement of 1,4-NQ ROS activity by select N-bases.** We next examine the
185 enhancement effect on 1,4-NQ using single N-base compounds. Figure 3a shows the DTT
186 consumption rate by 1,4-NQ in the presence of various amounts of 2-methylimidazole,
187 indicating the enhancement is linearly proportional to the amount of 2-methylimidazole. The
188 slope is then the enhancement factor per μmol of N-base: 66.8 pmol/min/ μg 1,4-NQ per μmol
189 of 2-methylimidazole. Five additional N-bases, including three more in the imidazole family
190 (imidazole, 4-methylimidazole and 2,4-dimethylimidazole) and two in the pyridine family
191 (pyridine and 3-methoxypyridine), were tested and all were found to enhance the 1,4-NQ
192 ROS activity. Their individual unit enhancement factors are listed in Table 2, ranging from
193 1.04 for 3-methoxypyridine to 91.2 pmol/min/ μg 1,4-NQ per μmol N-base for 2,4-
194 dimethylimidazole.

195 These N-bases exist in either the protonated (BH^+) or unprotonated form (B), and the
196 relative abundance of the two forms at the experimental pH condition (pH 7.40) depends on
197 their pK_a values. Both pK_a and the fraction of the unprotonated form (f_B) for the tested N-
198 bases are given in Table 2. As only the unprotonated form is effective in forming H-bonding
199 with 1,4-NQ, it is reasonable to normalize the unit enhancement factor against the amount of
200 the unprotonated form. Hereafter we term the unit enhancement factor normalized against the
201 unprotonated form B to be EF_B while the unit enhancement factor normalized against the sum

202 of B and BH⁺ to be apparent EF . The two are linked through f_B , i.e.,

$$203 \quad EF_B = \text{apparent } EF / f_B \quad (5)$$

204 EF_B ranges from 1.04 by 3-methoxypyridine to 921 pmol/min/(μg 1,4-NQ) per μmol N-base
205 for 2,4-dimethylimidazole.

206 It is noted that EF_B increases with pK_a among the six N-base compounds. The plot of
207 $\log(EF_B)$ vs. pK_a (Figure 4a) reveals a strong linear relationship between the two ($R^2 = 0.992$)
208 for the imidazole series. A larger pK_a value of the conjugated acid BH⁺ means higher basicity
209 of B, that is, the unprotonated form (i.e., B) has stronger ability to accept a proton from the
210 reductants. This agrees well with the observed results that the N-bases of larger pK_a values
211 have a stronger enhancement effect on 1,4-NQ and thereby lead to more DTT consumption.

212 The two tested pyridine N-bases have pK_a values lower than the imidazole N-bases.
213 Their enhancement effects were significantly smaller and only detectable at higher
214 concentrations ($> 10 \mu\text{mol}$). The linear increase in enhancing DDT consumption with
215 increasing pyridine N-base concentration only held up to the concentration of $\sim 100 \mu\text{mol}$,
216 beyond which the consumption of DTT increased at a much slower rate (Figure S2).

217 Histidine, an α -amino acid with an imidazole functional group, also shows a positive
218 effect on 1,4-NQ ROS activity. $6.4 \mu\text{mol}$ (1 mg) of histidine in the DTT assay yields an
219 enhancement effect between that of pyridine and imidazole at the same molar concentration,
220 which is consistent with the pK_a value of histidine (6.10) residing between pyridine (5.14)
221 and imidazole (6.95). Njus et al.³³ also found that the imidazole side-chain on histidine
222 residue can facilitate the proton-electron transfer from ascorbic acid to cytochrome b_{561} by
223 the formation of H-bonding in physiological conditions. However, as histidine is insoluble at
224 higher concentrations, it cannot be tested further in the DTT assay.

225 A second ROS active model compound, 9,10-phenanthrenequinone (9,10-PQ), was
226 also tested. The DTT consumption rate by 9,10-PQ in the absence of any N-bases was

227 measured to be ~ 9000 pmol/min/ μg , ~ 15 times larger than that of 1,4-NQ. Similarly, Li et
 228 al.³⁴ reported that 9,10-PQ has about 10 times higher ROS activity than 1,4-NQ in the DTT
 229 assay. DTT assays were also carried out on the mixtures of 9,10-PQ (0.015 μg) and varying
 230 amounts of imidazole (1.5-88 μmol). A linear relationship between $\Delta\text{DTT}_{9,10\text{-PQ}}$ and the
 231 amount of imidazole ($R^2 = 0.99$) was observed, yielding a slope of 267 pmol/min/(μg 9,10-
 232 PQ) / μmol imidazole, which produces a EF_B of 362 pmol/min/(μg 9,10-PQ) / μmol imidazole.
 233 This value is ~ 11 times larger than the EF_B of imidazole on 1,4-NQ (Table 2).

234 **Enhancement of HULIS ROS activity by N-bases.** We tested the DTT consumption of
 235 HULIS in the presence of various amounts of N-bases. As an example, Figure 3b shows the
 236 DTT consumption rate of HULIS (from ambient sample NS20091023) as a function of the
 237 amount of 2-methylimidazole. A clear linear relationship ($R^2 = 0.99$) is found, indicating a
 238 similar pattern as seen in Figure 3a showing the enhancement effect by 2-methylimidazole on
 239 1,4-NQ ROS activity. The apparent EF values as determined by the slope and EF_B computed
 240 using Eq (5) for all the six N-bases are summarized in Table 2. Again, $\log(EF_B)$ is linearly
 241 proportional to pK_a for the imidazole series (Figure 4a). For each of the tested N-bases, the
 242 EF_B acting on HULIS is much smaller (67-308 times smaller) than that acting on 1,4-NQ.
 243 HULIS is a mixture and only some of its constituents (such as quinones) have DTT activity,
 244 hence, a smaller enhancement effect on per unit mass HULIS than that on 1,4-NQ is expected.
 245 It is also possible that the redox active constituents in HULIS are less sensitive than 1,4-NQ
 246 to the hydrogen bonding effect by the N-bases, which is demonstrated above by the EF_B with
 247 imidazole acting on 1,4-NQ and 9,10-PQ differing by a factor of ~ 11 .

248 The quantitative relationship of $\log(EF_B)$ vs. pK_a for the imidazole series allows the
 249 calculation of the apparent EF at the physiological pH 7.40 for an imidazole derivative of a
 250 given pK_a :

$$251 \quad \text{apparent } EF = EF_B \times f_B = 10^{(m \times pK_a + c)} \times \frac{1}{1 + [H^+]/K_a} \quad (6)$$

252 where m is the slope and c is the intercept of the $\log (EF_B)$ vs. pK_a . Figure 4b shows the
253 calculated apparent EF by the imidazole series acting on HULIS (red) and 1,4-NQ (green) in
254 the pK_a range of 4-10. With the minimum detectable enhancement factor at ~ 0.01
255 $\mu\text{mol}/\text{min}/\mu\text{g}$ (HULIS) per μmol N-base, the imidazole derivatives with a pK_a larger than ~ 6
256 have a measurable enhancement effect on HULIS-mediated ROS generation. At pK_a of 9.4 or
257 higher, the unprotonated N-base fraction would be reduced to $<1\%$, thereby limiting the
258 enhancement effect. Within the imidazole series, pK_a increases with increasing carbon
259 number in the alkyl substituents.³⁵ Alkyl imidazole homologues (C_6 - C_{13}) observed in
260 atmospheric HULIS are estimated to have pK_a in the range of 7.2-9.0 using the pK_a -structure
261 relationships developed for alkyl imidazoles by Lenarcik and Ojczenasz.³⁵ Calculations of
262 apparent EF by Eq. (6) predict that this range of alkyl imidazoles would be 1.6-5 times more
263 effective than imidazole in facilitating HULIS-mediated ROS generation under the
264 physiological pH condition.

265 Only two compounds in the pyridine series were tested for their effect on HULIS-
266 mediated ROS generation. The weaker pyridine series EF_B acting on HULIS is consistent
267 with their lower pK_a than the imidazole series (Table 2). The EF measurements, although
268 limited, suggest that the pyridine series may represent a different $\log (EF_B)$ vs. pK_a
269 relationship than the imidazole series (Figure 4a). Additional experiments with more pyridine
270 compounds are needed to verify this.

271 **Enhancement effect of imidazole on ROS activity mediated by different ambient**
272 **HULIS samples.** The enhancement effect of N-bases on different ambient HULIS samples
273 was also examined for qualitative evaluation of the variability in ROS active components.
274 Figure 5 compares DTT consumption rate by HULIS from six ambient samples in the
275 absence and presence of imidazole ($15 \mu\text{mol}$). The samples were selected from a pool of
276 ~ 120 samples collected at two locations in the PRD in different seasons. Our source

277 apportionment study using positive matrix factorization analysis of PM_{2.5} major constituents
278 and organic tracers in the samples has identified secondary formation, biomass burning and
279 ship emissions as the major contributing sources to HULIS.³⁶ Taking advantage of the source
280 apportionment results, we selected two samples having a dominant secondary formation
281 contribution, one sample dominated by biomass burning HULIS and three samples dominated
282 by HULIS associated with ship emissions. The enhancement of HULIS-mediated ROS
283 activity by imidazole was invariably observed for all the HULIS samples. The redox
284 activities of ambient HULIS increased by 14% from 6.4 ± 1.2 in the absence of imidazole to
285 7.2 ± 1.2 pmol DTT/min per μg HULIS in the presence of 15 μmol of imidazole. The EF_B
286 value was on average 0.078 ± 0.018 and ranged from 0.049 to 0.104 pmol/min/ μg HULIS per
287 μmol imidazole. The two samples dominated by HULIS associated with secondary formation
288 had higher EF_B than the other samples (Figure 5). However, due to the small number of
289 samples tested, it is uncertain whether this observation suggests that HULIS of secondary
290 origin contains more ROS active constituents that are sensitive to enhancement by N-bases.

291 A logical inference arises from the discovery of imidazoles and pyridines enhancing ROS
292 activity in HULIS samples. That is, ROS activity of atmospheric HULIS measured as the
293 DTT consumption rate in pmol/min/ μg HULIS would be higher in DTT assays performed
294 with higher HULIS doses since more of the N-bases would be available to enhance the ROS
295 production mediated by HULIS in the samples of higher HULIS doses. We report in our
296 previous study the DTT consumption data in pmol/min as a function of HULIS dose (μg) in
297 the incubation solution (Figure 2a in Lin and Yu¹⁵). A close examination of the data suggests
298 that the DTT consumption at higher HULIS dose deviated upwards from the linear curve
299 established by the lower dose data. A quadratic curve of zero intercept yields excellent fitting
300 with all the data in the full range of the tested HULIS doses ($y=0.44 x^2+9.38 x$, $r^2 = 0.999$)
301 (Figure 6), indicating the DTT consumption rate per μg HULIS increases with HULIS dose.

302 The dependence of the DTT consumption rate per μg HULIS on the HULIS-dose could also
303 be discerned if we fit the lower-dose and the higher-dose data with two separate linear curves,
304 which produces a slope of 10.5 and 15.4 $\text{pmol}/\text{min}/\mu\text{g}$ HULIS, respectively (Figure 6). This
305 result is consistent with the characteristics of HULIS containing both ROS active constituents
306 and components enhancing ROS activities.

307 **Implications on health effects of PM.** Atmospheric HULIS contains both redox active
308 components and redox inactive constituents such as heterocyclic N-containing bases. The
309 DTT assay performed on the atmospheric HULIS fraction in the presence of imidazoles
310 clearly indicates that the redox activity of the HULIS fraction is enhanced by the co-existing
311 redox inactive N-bases. As such, the ROS response of HULIS, perhaps PM by extension, is
312 not linear to the dose. Once inhaled, the redox activity exerted by HULIS in PM could also be
313 enhanced by histidine residues, which contain imidazole side chains that have a $pK_a \sim 6$. This
314 work reveals the health effect implications of N-bases present in atmospheric PM and
315 underlines the importance of characterizing the molecular level of the redox active
316 components and the redox inactive N-bases in the HULIS fraction.

317

318 **Acknowledgements**

319 This study was supported by the Research Grants Council of Hong Kong (621510 and
320 621312). We thank Professor Quan Shi and Mr. Bin Jiang at China Petroleum University for
321 obtaining the FTICR-MS data of the HULIS samples.

322 **Supporting Information**

323 Two supporting figures showing DDT consumption rate in response to pyridines and ultra-
324 high resolution mass spectrometric data of N- containing compounds in biomass burning
325 source samples and an ambient sample. This material is available free of charge via the
326 Internet at <http://pubs.acs.org>.

327

328 **References**

329 (1) Nation Research Council (NRC). *Research Priorities for Airborne Particulate Matter. I.*
330 *Immediate Priorities and a Long-range Research Portfolio*; National Academy Press: Washington,

- 331 DC, 1998.
- 332 (2) Zanobetti, A.; Schwartz, J.; Dockery, D. W. Airborne particles are a risk of factor for hospital
333 admissions for heart and lung disease. *Environ. Health Perspect.* **2000**, *108*, 1071–1077.
- 334 (3) Breysse, P. N.; Delfino, R. J.; Dominici, F.; Elder, A. C. P.; Frampton, M. W.; Froines, J. R.; Geyh,
335 A. S.; Godleski, J. J.; Gold, D. R.; Hopke, P. K.; Koutrakis, P.; Li, N.; Oberdörster, G.; Pinkerton,
336 K. E.; Samet, J. M.; Utell, M. J.; Wexler, A. S. US EPA particulate matter research centers:
337 Summary of research results for 2005-2011. *Air Qual. Atmos. Health* **2013**, *6*, 333–355.
- 338 (4) Gurgueira, S. A.; Lawrence, J.; Coull, B.; Murthy, G. G. K.; González-Flecha, B. Rapid increase in
339 the steady-state concentration of reactive oxygen species in the lungs and heart after particulate air
340 pollution inhalation. *Environ. Health Perspect.* **2002**, *110*, 749–755.
- 341 (5) González-Flecha, B. Oxidant mechanisms in response to ambient air particles. *Mol. Aspects Med.*
342 **2004**, *25*, 169–182.
- 343 (6) Di Pietro, A.; Visalli, G.; Munao, F.; Baluce, B.; La Maestra, S.; Primerano, P.; Corigliano, F.; De
344 Flora, S. Oxidative damage in human epithelial alveolar cells exposed in vitro to oil fly ash
345 transition metals. *Int. J. Hyg. Environ. Health* **2009**, *212*, 196–208.
- 346 (7) Verma, V.; Polidori, A.; Schauer, J. J.; Shafer, M. M.; Cassee, F. R.; Sioutas, C. Physicochemical
347 and toxicological profiles of particulate matter in Los Angeles during the October 2007 Southern
348 California wildfires. *Environ. Sci. Technol.* **2009**, *43*, 954–960.
- 349 (8) Pritchard, R. J.; Ghio, A. J.; Lehmann, J. R.; Winsett, D. W.; Tepper, J. S.; Park, P.; Gilmour, M. I.;
350 Dreher, K. L.; Costa, D. L. Oxidant generation and lung injury after particulate air pollutant
351 exposure increase with the concentrations of associated metals. *Inhalation Toxicol.* **1996**, *8*, 457–
352 477.
- 353 (9) Prahalad, A. K.; Inmon, J.; Dailey, L. A.; Madden, M. C.; Ghio, A. J.; Gallagher, J. E. Air
354 pollution particles mediated oxidative DNA base damage in a cell free system and in human
355 airway epithelia cells in relation to particulate metal content and bioreactivity. *Chem. Res. Toxicol.*
356 **2001**, *14*, 879–887.
- 357 (10) See, S. W.; Wang, Y. H.; Balasubramanian, R. Contrasting reactive oxygen species and
358 transition metal concentrations in combustion aerosols. *Environ. Res.* **2007**, *103*, 317–324.
- 359 (11) Charrier, J. G.; Anastasio, C. On dithiothreitol (DTT) as a measure of oxidative potential for
360 ambient particles: Evidence for the importance of soluble transition metals. *Atmos. Chem. Phys.*
361 **2012**, *12*, 9321–9333.
- 362 (12) Saffari, A.; Daher, N.; Shafer, M. M.; Schauer, J. J.; Sioutas, C. Global perspective on the
363 oxidative potential of airborne particulate matter: A synthesis of research findings. *Environ. Sci.*
364 *Technol.* **2014**, *48*, 7576–7583.
- 365 (13) Kumagai, Y.; Arimoto, T.; Shinyashiki, M.; Shimojo, N.; Nakai, Y.; Yoshikawa, T.; Sagai, M.
366 Generation of reactive oxygen species during interaction of diesel exhaust particle components
367 with NADPH-cytochrome P450 reductase and involvement of the bioactivation in the DNA

- 368 damage. *Free Radical Biol. Med.* **1997**, *22*, 479–487.
- 369 (14) Graber, E. R.; Rudich, Y. Atmospheric HULIS: How humic-like are they? A comprehensive
370 and critical review. *Atmos. Chem. Phys.* **2006**, *6*, 729–753.
- 371 (15) Lin, P.; Yu, J. Z. Generation of reactive oxygen species mediated by humic-like substances in
372 atmospheric aerosols. *Environ. Sci. Technol.* **2011**, *45*, 10362–10368.
- 373 (16) Verma, V.; Rico-Martinez, R.; Kotra, N.; King, L.; Liu, J.; Snell, T. W.; Weber, R. J.
374 Contribution of water-soluble and insoluble components and their hydrophobic/hydrophilic
375 substances to the reactive oxygen species-generating potential of fine ambient aerosols. *Environ.*
376 *Sci. Technol.* **2012**, *46*, 11384–11392.
- 377 (17) Lin, P.; Rincon, A. G.; Kalberer, M.; Yu, J. Z. Elemental composition of HULIS in the Pearl
378 River Delta Region, China: Results inferred from positive and negative electrospray high
379 resolution mass spectrometric data. *Environ. Sci. Technol.* **2012**, *46*, 7454–7462.
- 380 (18) Laskin, A.; Smith, J. S.; Laskin, J. Molecular characterization of nitrogen-containing organic
381 compounds in biomass burning aerosols using high-resolution mass spectrometry. *Environ. Sci.*
382 *Technol.* **2009**, *43*, 3764–3771.
- 383 (19) Brielmann, H. L.; Kaufman, P. B.; Duke, J. A.; Cseke, L. J.; Warber, S. L.; Kirakosyan, A.
384 *Natural products from plants*, 2nd ed.; CRC Press: New York, 2006.
- 385 (20) De Haan, D. O.; Tolbert, M. A.; Jimenez, J. L. Atmospheric condensed-phase reactions of
386 glyoxal with methylamine. *Geophys. Res. Lett.* **2009**, *36*, L11819–L11824.
- 387 (21) De Haan, D. O.; Hawkins, L. N.; Kononenko, J. A.; Turley, J. J.; Corrigan, A. L.; Tolbert, M.
388 A.; Jimenez, J. L. Formation of nitrogen-containing oligomers by methylglyoxal and amines in
389 simulated evaporating cloud droplets. *Environ. Sci. Technol.* **2011**, *45*, 984–991.
- 390 (22) Sedehi, N.; Takano, H.; Blasic, V. A.; Sullivan, K. A.; De Haan, D. O. Temperature- and pH-
391 dependent aqueous-phase kinetics of the reactions of glyoxal and methylglyoxal with atmospheric
392 amines and ammonium sulfate. *Atmos. Environ.* **2013**, *77*, 656–663.
- 393 (23) Kumagai, Y.; Koide, S.; Taguchi, K.; Endo, A.; Nakai, Y.; Yoshikawa, T.; Shimojo, N.
394 Oxidation of proximal protein sulfhydryls by phenanthraquinone, a component of diesel exhaust
395 particles. *Chem. Res. Toxicol.* **2002**, *15*, 483–489.
- 396 (24) Kipp, B. H.; Faraj, C.; Li, G. L.; Njus, D. Imidazole facilitates electron transfer from organic
397 reductants. *Bioelectrochem.* **2004**, *64*, 7–13.
- 398 (25) Lin, P.; Huang, X. F.; He, L. Y.; Yu, J. Z. Abundance and size distribution of HULIS in
399 ambient aerosols at a rural site in South China. *J. Aerosol Sci.* **2010**, *41*, 74–87.
- 400 (26) Lin, P.; Engling, G.; Yu, J. Z. Humic-like substances in fresh emissions of rice straw burning
401 and in ambient aerosols in the Pearl River Delta Region, China. *Atmos. Chem. Phys.* **2010**, *10*,
402 6487–6500.
- 403 (27) Bones, D. L.; Henricksen, D. K.; Mang, S. A.; Gonsior, M.; Bateman, A. P.; Nguyen, T. B.;
404 Cooper, W. J.; Nizkorodov, S. A. Appearance of strong absorbers and fluorophores in limonene-O₃

- 405 secondary organic aerosol due to NH_4^+ -mediated chemical aging over long time scales. *J. Geophys.*
406 *Res.* **2010**, *115*, D05203.
- 407 (28) Shinyashiki, M.; Eiguren-Fernandez, A.; Schmitz, D. A.; Di Stefano, E.; Li, N.; Linak, W. P.;
408 Cho, S. H.; Froines, J. R.; Cho, A. K. Electrophilic and redox properties of diesel exhaust particles.
409 *Environ. Res.* **2009**, *109*, 239–244.
- 410 (29) Kendrick, E. A mass scale based on $\text{CH}_2 = 14.0000$ for high resolution mass spectrometry of
411 organic compounds. *Anal. Chem.* **1963**, *35*, 2146–2154.
- 412 (30) Hughey, C. A.; Hendrickson, C. L.; Rodgers, R. P.; Marshall, A. G.; Qian, K. N. Kendrick
413 mass defect spectrum: A compact visual analysis for ultrahigh-resolution broadband mass spectra.
414 *Anal. Chem.* **2001**, *73*, 4676–4681.
- 415 (31) Bilow, N.; Ralph, D. H. Method of making an epoxy prepolymer curing agent. *U.S. Patent*
416 **1985**, 4, 534, 882.
- 417 (32) R. Williams. pKa Data Compiled by R. Williams;
418 research.chem.psu.edu/brpgroup/pKa_compilation.pdf
- 419 (33) Njus, D.; Wagle, M.; Kelley, P. M.; Kipp, B. H.; Schlegel, H. B. Mechanism of ascorbic acid
420 oxidation by cytochrome b_{561} . *Biochemistry* **2001**, *40*, 11905–11911.
- 421 (34) Li, Q. F.; Wyatt, A.; Kamens, R. M. Oxidant generation and toxicity enhancement of aged-
422 diesel exhaust. *Atmos. Environ.* **2009**, *43*, 1037–1042.
- 423 (35) Lenarcik, B.; Ojczenasz, P. The influence of the size and position of the alkyl groups in
424 alkyimidazole molecules on their acid-base properties. *J. Heterocyclic Chem.* **2002**, *39*, 287–290.
- 425 (36) Kuang, B. Y.; Lin, P.; Huang, X. H. H.; Yu, J. Z. Sources of humic-like substances in the
426 Pearl River Delta, China: Positive matrix factorization analysis of $\text{PM}_{2.5}$ major components and
427 source markers. *Atmos. Chem. Phys. Discuss.* **2014**, *14*, 23913–23947.

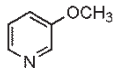
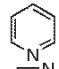
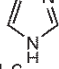
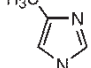
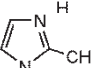
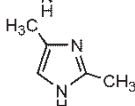
Table 1. Composition combinations in the DTT assays that involve redox inactive N-bases and redox reactive single components or HULIS mixtures ^a.

assay No.	N-base (100 μ L)	ROS active component (100 μ L)						
1.1-1.6	3-methoxypyridine (μ L/mL) ^b	0	10	50	100	150	200	
2.1-2.6	pyridine (μ L/mL) ^b	0	10	50	100	150	200	3 μ g/mL 1,4-NQ
3.1-3.6	imidazole (mg/mL)	0	1	10	20	30	40	
4.1-4.6	4-methylimidazole (mg/mL)	0	1	5	10	15	20	or
5.1-5.6	2-methylimidazole (mg/mL)	0	1	5	10	15	20	50-150 μ g/mL HULIS
6.1-6.6	2,4-dimethylimidazole (mg/mL)	0	1	5	10	15	20	

^a Each 200 μ L sample consists of 100 μ L aqueous solution of a certain N-base of different concentrations and 100 μ L solution of an ROS active component (either 1,4-NQ or HULIS). The incubation time was 30 min for assays involving 1,4-NQ and 90 min for assays involving HULIS.

^b 3-methoxypyridine and pyridine are liquid. Their solutions were prepared in the unit of μ L/mL.

Table 2. Nitrogen base compounds tested and their unit enhancement factor to ROS activities by 1,4-NQ and an ambient HULIS sample.

Nitrogen Compound	Chemical Structure	pKa Value ^a	f_B ^b	N-base acting on 1,4-NQ (pmol/min/ μ g per μ mol N-base) ^c		N-base acting on HULIS (pmol/min/ μ g per μ mol N-base)	
				Apparent EF	EF_B	Apparent EF	EF_B
3-methoxy pyridine		4.88	0.997	1.04	1.04	0.0155	0.0155
pyridine		5.14	0.994	1.74	1.75	0.0108	0.0109
imidazole		6.95	0.738	23.4	31.7	0.0772	0.105
4-methyl imidazole		7.45	0.471	63.4	135	0.206	0.437
2-methyl imidazole		7.75	0.309	66.8	216	0.256	0.828
2,4-dimethyl imidazole		8.36	0.099	91.2	921	0.335	3.38

^a The pK_a value of 2,4-dimethylimidazole is obtained from Bilow and Hermansen³¹ and all the other compounds are from Williams³².

^b f_B is the fraction of the unprotonated form of each N-base in the solution of pH 7.40.

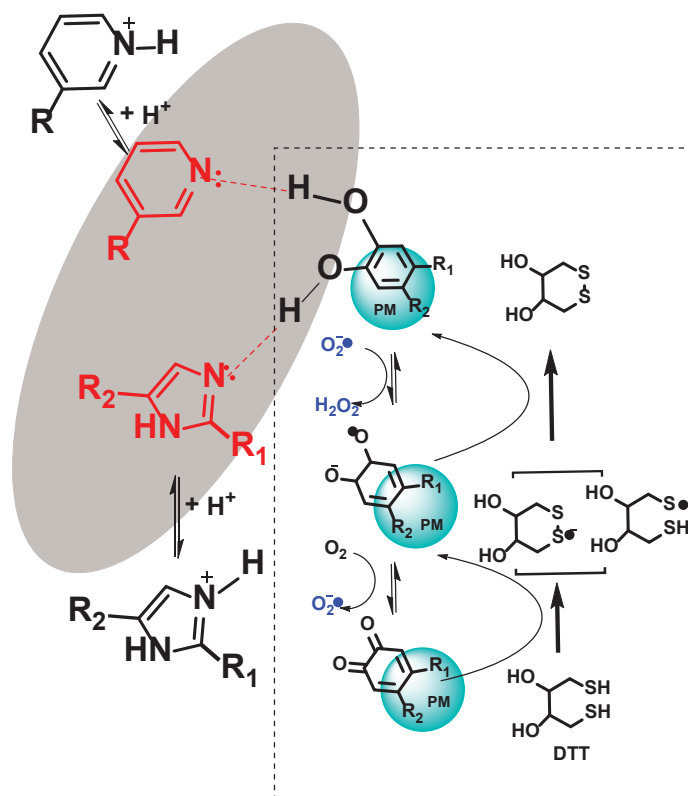


Figure 1. Conceptual diagram of quinone-catalyzed ROS production and concomitant consumption of DTT (in the box), with imidazole and pyridine compounds facilitating the oxidation of hydroquinone to semi-quinone through H-bonding.

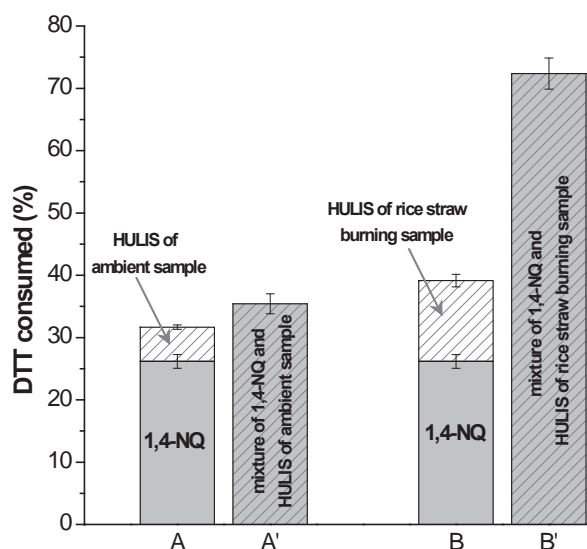


Figure 2. Comparison of DTT consumption by 1,4-NQ (3 $\mu\text{g}/\text{mL}$) and HULIS (60 $\mu\text{g}/\text{mL}$) samples individually and their mixtures. Column A is the DTT response from separate solutions of 1,4-NQ and HULIS from the NS20091023 ambient sample, while column A' represents the DTT response from the mixture of 1,4-NQ and HULIS. Similarly, column B is the DTT response from separate solutions of 1,4-NQ and HULIS from the rice straw burning sample and column B' represents the DTT response from the mixture of the two. The incubation time was 30 min in these experiments. The error bars represent the standard deviations of triplicate measurements.

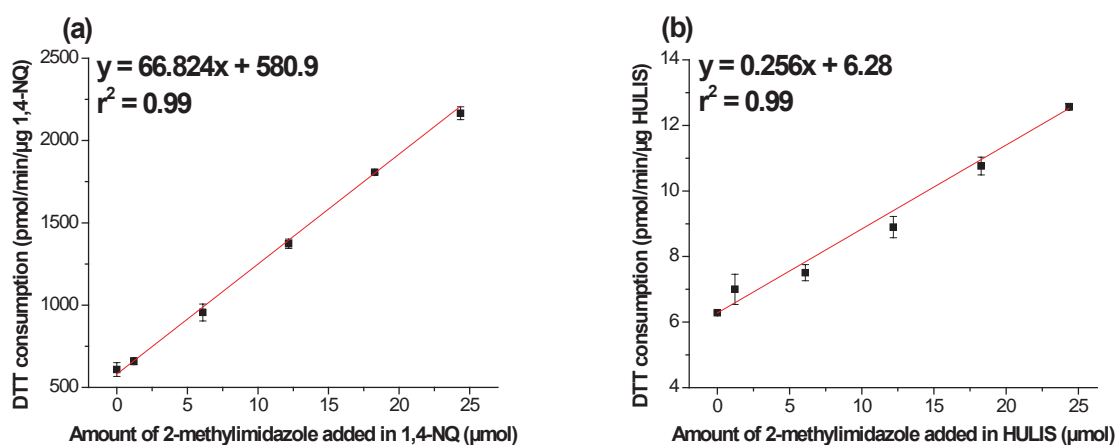


Figure 3. DTT consumption rate by (a) 1,4-NQ and (b) HULIS in the presence of various amounts of 2-methylimidazole. The error bars represent the standard deviations of triplicate measurements. HULIS used in (b) was extracted from the ambient aerosol sample NS20091023.

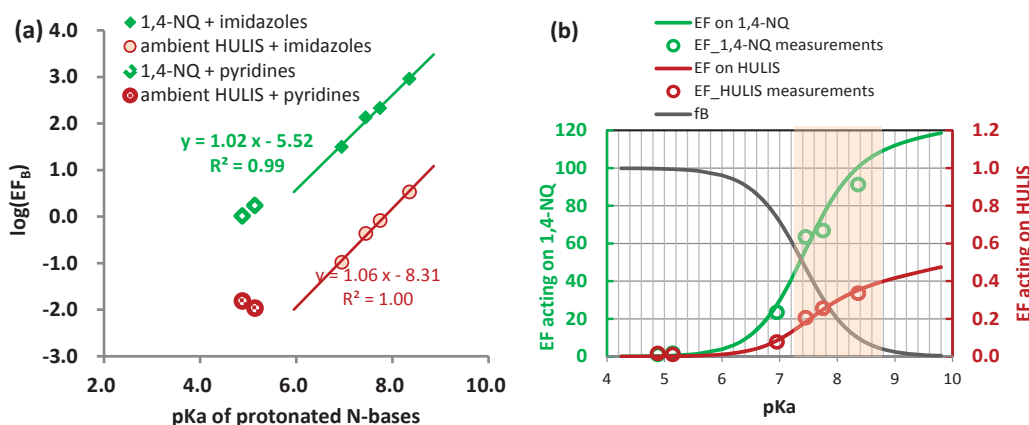


Figure 4. (a) Correlation of $\log(EF_B)$ against pK_a of the protonated N-bases. EF_B is the unit enrichment factor normalized against the unprotonated form. (b) The predicted enrichment factor (normalized against the total N-base) acting on 1,4-NQ and ambient HULIS for imidazole homologues. The fraction of the unprotonated form (f_B) at physiological pH 7.4 is also shown as a function of pK_a .

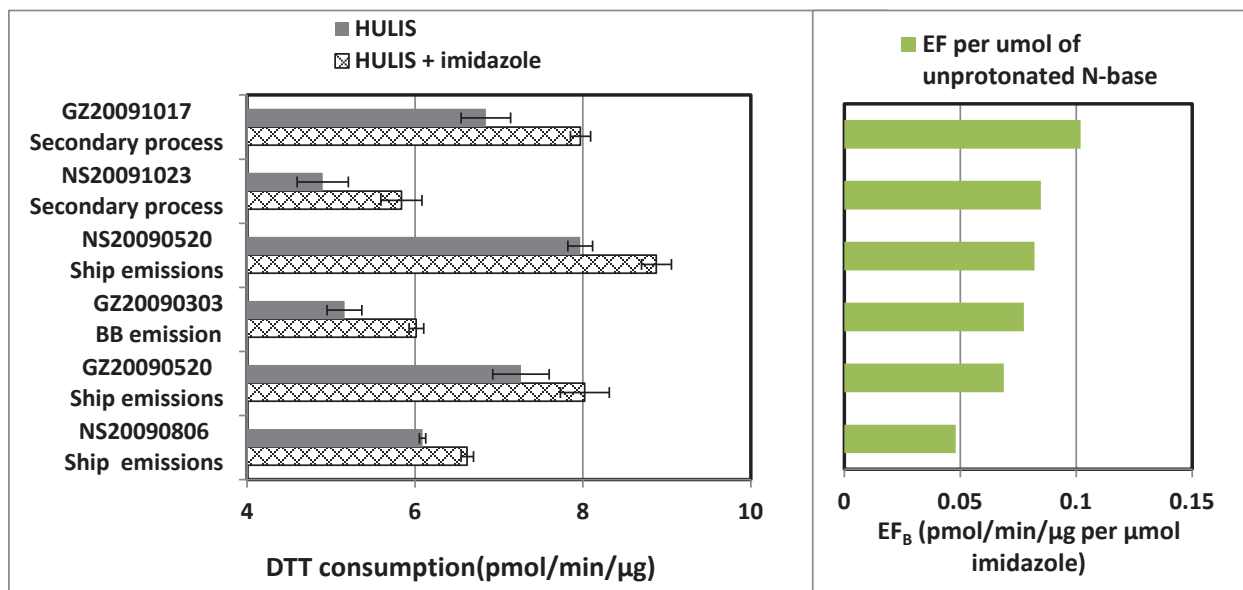


Figure 5. Comparison of DTT consumption rate by HULIS from different ambient samples in the absence and presence of imidazole (15 μmol). The error bars represent the standard deviations of triplicate measurements. The right plot shows the EF_B of imidazole acting on the six ambient HULIS samples order from high to low.

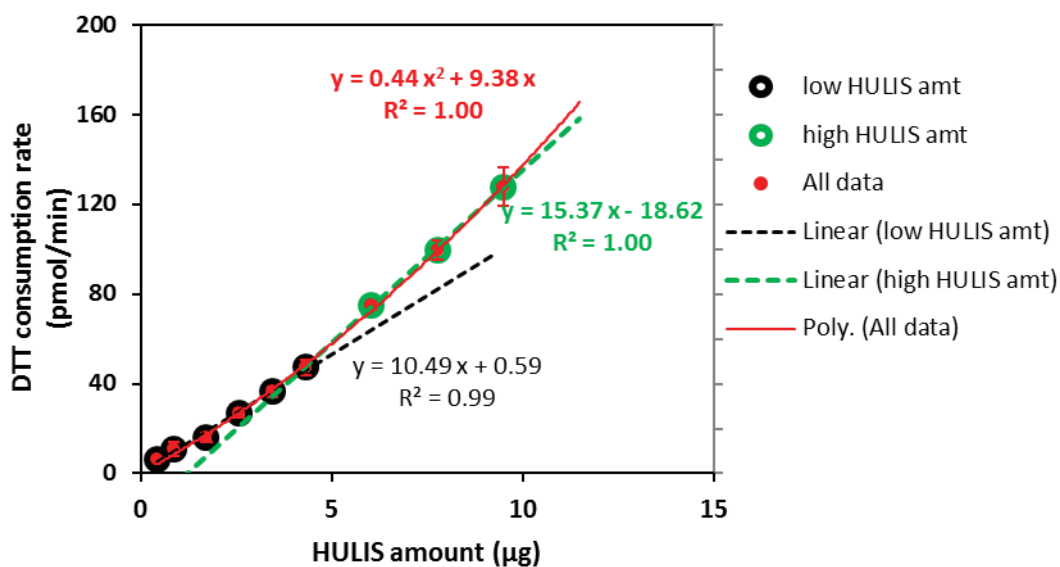


Figure 6. DTT consumption rate as a function of HULIS amount used in the assay. The original data was shown in Figure 2b in the paper by Lin and Yu (2011). Error bars represent the standard variations of triplicate measurements.

TOC graphic:

